

7th CIRP Conference on Surface Integrity

Machining Effect On The Surface Integrity And SE Of Additively Manufactured And Heat-Treated Nitinol

Rachele Bertolini^a, Saeed Khademzadeh^b, Andrea Ghiotti^a, Stefania Bruschi^a

^aDepartment of Industrial Engineering, University of Padova, Via Venezia 1, 35131, Padova, Italy

^bDepartment of Manufacturing Processes, RISE research institutes of Sweden, Argongatan 30, 431 53, Mölndal, Sweden

* Corresponding author. Tel.: +049-827 6818. E-mail address: rachele.bertolini@unipd.it

Abstract

Nitinol belongs to the class of smart materials that have attracted the attention of researchers in recent decades due to their new promising industrial applications. Because of the austenite/martensite phase transformation, nitinol offers unique properties: superelasticity and shape memory effect. The former ability can be exploited for sensing, actuating, and damping applications. On the other hand, additive manufacturing of nitinol has started kicking off unimaginable applications exploiting the complexity-for-free characteristics offered by the 3D printing processes. Although stand-alone research on additive manufacturing of nitinol is available, the impact of different manufacturing steps, such as machining and heat treatment, on its superelasticity is severely lacking.

This work used a powder bed fusion process using a laser beam to manufacture a Ni_{50.4}Ti_{49.6} austenitic alloy, which was subsequently heat-treated at different aging temperatures. Subsequently, turning operations were carried out at varying cutting speeds under cryogenic cooling conditions. An in-depth characterization of the surface integrity and SE alterations induced by manufacturing was conducted before and after machining. The outcome of the work provides the best combination of heat treatment and machining parameters that allow for maximum surface integrity and SE.

© 2024 The Authors. Published by Elsevier B.V.

This is an open access article under the CC BY-NC-ND license (<https://creativecommons.org/licenses/by-nc-nd/4.0>)

Peer-review under responsibility of the scientific committee of the 7th CIRP Conference on Surface Integrity

Keywords: Nitinol; Machining; Surface integrity; Superelasticity

1. Introduction

Nitinol (NiTi) belongs to the category of shape memory alloys (SMA) characterized by two unique properties, namely superelasticity (SE) and shape memory effect (SME) [1]. These fascinating characteristics make them suitable for various pioneering applications in the automotive, military, aerospace, and biomedical fields.

Fig. 1 shows the NiTi mechanical behavior as a function of the temperature, focusing on the SME, SE, and plastic deformation phenomena. When NiTi is in the austenitic phase, namely at the origin point *O*, it can be loaded along the path *O*->*E* provoking a stress-induced transformation to the martensitic state. Upon unloading, the material transforms back to an austenitic state, and the superelastic deformation is

recovered. A considerably high elastic strain in the order of 11% can be achieved in such conditions.

When NiTi is cooled down below martensite finish temperature (*M_f*), a complete transformation from austenite to martensite occurs (*O*->*A*). The material is deformed through reorientation and detwinning of martensite (*A*->*B*).

Then, the load releasing causes the elastic unloading of the reoriented detwinned martensite, and the material remains deformed. On heating above the austenite finish temperature (*A_f*), the material transforms from martensite to austenite and recovers the pseudoelastic deformation remembering its former shape.

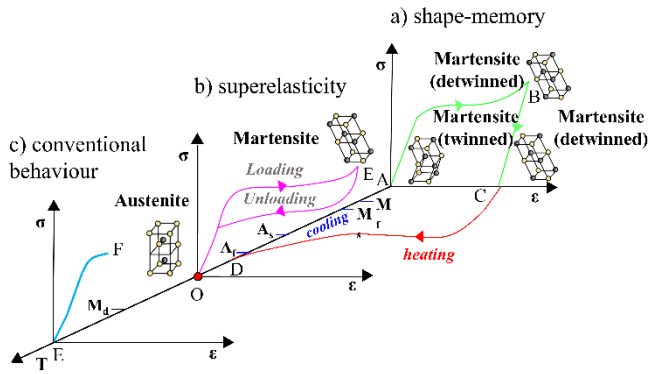


Figure 1. Stress-strain curves of NiTi as a function of temperature: a) shape memory, b) SE, and c) conventional behavior [1,2].

When the temperature exceeds the martensite deformation temperature (M_d), NiTi behaves as a conventional metal, namely with a standard elastoplastic deformation (E- \rightarrow F).

In general, the M_d values of NiTi alloys vary with the phase transformation temperatures, which are mainly affected by the Ni content and type of heat treatment [3].

For example, the M_d of the Ni₅₆Ti₄₄ alloy is approximately 150 °C, according to [3].

Machinability of Nitinol is still considered a very challenging task due to its unconventional stress-strain characteristics (Fig. 1), low thermal conductivity, and low elastic modulus. These factors are responsible for severe tool wear and high specific cutting energy, but they may also adversely affect the surface integrity characteristics of the finished product. In turn, machining-induced subsurface microstructure and phase transformation are of great importance because they influence the functional performance of NiTi parts.

In [4], the Ni_{50.95}Ti_{49.05} room-temperature austenitic alloy was machined at various cutting speeds ($V=10$ m/min, $V=25$ m/min, $V=50$ m/min, $V=100$ m/min) under both non-preheating and preheating conditions. Temperature measurements showed that the workpiece did not exceed the M_d at any of the considered cutting speeds under the non-preheating condition, while it did under the preheating one. After machining under the non-preheating condition, XRD measurements showed a decrease in the austenite intensity peak, less remarkable at increasing cutting speed. Contrarily, the intensity of martensite decreased slightly with the cutting speed increase. After machining under the preheating condition, the intensity of the diffraction peak of the austenite phase decreased, and peak broadening and peak shifting occurred, nevertheless, no pronounced martensite peak was observed.

In [5], a room temperature austenitic NiTi alloy ($A_f=-11^\circ\text{C}$) was machined at varying cutting speeds, namely adopting $V=12.5$ m/min, $V=25$ m/min, $V=50$ m/min, under dry, minimum quantity lubrication (MQL) and cryogenic cooling conditions. The increasing cutting speed provoked a broadening of the XRD austenitic peaks, while the opposite behavior was registered at low cutting speed. At low cutting speed, the mechanical effects were dominant over the thermal ones leading to an increase of dislocation density and defects in the microstructure of the machined surface, hence reducing SE. Comparing different lubricating cooling conditions, it was

evident that the cryogenic cooling induced peak broadening and martensite formation.

Even if negatively affecting the SE, cryogenic machining was reported to yield positive effects in terms of surface roughness as well as tool wear reduction when turning NiTi.

In [6], it was shown indeed that cryogenic machining of NiTi can reduce the tool wear since the material becomes martensitic, hence softer for the considered NiTi alloy, when cut.

Recently, additive manufacturing (AM) of NiTi has grown in interest among researchers thanks to its high flexibility and freeform capability, opening new opportunities for SMA applications. Nevertheless, the AM microstructure greatly differs from those of metallic components obtained from conventional manufacturing processes, like rolling, forging, and casting, hence a different machinability response of AM NiTi can be expected. Nevertheless, the machinability of AM NiTi has not been studied so far, except in a previous study by the Authors [7]. In this work, the machinability of an AM NiTi alloy was investigated at fixed cutting speed under flood and cryogenic cooling conditions showing that the latter was capable of improving the surface integrity thanks to the formation of a smoother and harder surface.

On this basis, an additional contribution to the effect of machining parameters on surface integrity and SE of NiTi is required. In this framework, a room-temperature austenitic NiTi alloy was additively manufactured through the laser power bed fusion process (PBF-L) and, subsequently, heat treated to enhance the SE of the base material. The turning operations were conducted under cryogenic conditions to explore the metal machinability at varying cutting speeds. The transformation temperatures, nano-hardness, microstructure, and surface topography were taken into consideration and correlated to the NiTi microstructure of both the as-built and heat-treated conditions.

2. Materials and methods

2.1. Sample fabrication

Ni_{50.4}Ti_{49.6} (at%) powders with spherical shape (Fig. 2a) were utilized in this study. The particles (15-45 μm size range) were produced via argon atomization with nominal chemical composition reported in Fig 2b. The PBF-LB process was performed on a MYSINT™ 100 machine using a fiber laser with a maximum power of 200 W and a laser spot of 30 μm . The PBF-LB process was carried out in an argon atmosphere with an oxygen level below 100 ppm to reduce oxidation during the process.

NiTi cylinders of 10 mm diameter and 40 mm height were printed vertically on a titanium platform using the island scanning strategy and remelting of initial layers.

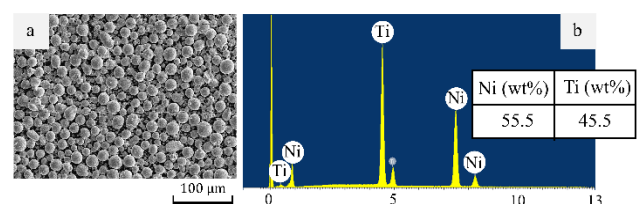


Fig. 2. a) SEM image of the NiTi powders and b) EDS spectra from a).

The PBF-LB parameters were set as follows: laser power 70 W, scanning speed 1100 mm/s, hatch distance 0.06 mm, layer thickness 0.025 mm.

According to the parameters described, the input energy densities settled at 42.42 J/mm³. This set of parameters was identified as the optimal one in a screening study as it offered the highest density as well as a single-phase austenitic microstructure at room temperature [8]. Afterward, a batch of PBF-LB samples was heat treated to enhance SE and relieve stresses induced by the PBF-LB process. Specifically, the samples were first subjected to a solution treatment at 1060 °C for 60 min and rapidly cooled in water. Then, they were subjected to aging treatment at T = 600 °C (T6) for 180 min, followed by air cooling.

2.2. Machining trials

As-built (AB) and T6 PBF-LB NiTi samples were turned on a Mori Seiki™ CNC lathe. The cutting tools were the VCEX 110301L-F 1125 inserts by Sandvik Coromant™, characterized by a radius of 0.1 mm, a rake angle of 5.3° and a flank angle of 7°. The tool grade is a PVD (TiAlN+TiAlN) coated 1125 WC, suitable for cutting difficult-to-cut materials like NiTi alloys. Before usage, each tool was inspected with a FEI™ Quanta 400 Scanning Electron Microscope (SEM) to ensure the absence of manufacturing flaws, and a fresh tool was used for each cutting condition.

The machining trials consisted of longitudinal turning of the AM cylinders, which were previously rough-turned to remove their external skin. The finishing cutting parameters were chosen from the tool manufacturer's datasheet. In particular, the cutting depth and the feed were kept constant and equal to 0.25 mm and 0.07 mm/rev, respectively. The cutting speed (V) was varied, using V=31 m/min, V=62 m/min, and to V=93 m/min. Machining was carried out under cryogenic cooling conditions, based on promising results of a previous study [7] where cryogenic machining carried out on wrought NiTi was proved to represent a suitable strategy to increase the Nitinol surface integrity. Details about the adopted cryogenic apparatus can be found in a previous work of the Authors [9].

2.3. Sample characterization after fabrication and machining

For metallographic investigations, the samples were cut, hot mounted, ground using up to 4000 grit SiC paper and polished using a synthetic cloth with 1 μm diamond suspension. After polishing, the PBF-LB sections were chemically etched with HF (1 mL), HNO₃ (2 mL), and water (47 mL) solution for 70 seconds to reveal the grain boundaries. The optical microscope Leica™ DMRE equipped with a high-definition digital camera

and the SEM were utilized for the microstructural characterization.

Differential scanning calorimeter (DSC) analyses were carried out using a DSC Q200™ machine to determine the NiTi characteristic transformation temperatures TTs.

The evaluation of the mechanical properties of the PBF-LB samples was achieved via the Ultrananoindenter UNHT by Anton Paar™ equipped with a pyramidal Berkovich tip. Nanoindentations were carried out by using a load of 1 mN, which was applied at a rate of 2 mN/min and kept constant for 10 seconds to stabilize the time-dependent deformation, then released at the same rate. At least twenty random indentations per section were carried out and the average value was computed.

All the above-mentioned analyses have been carried out on the samples before and after heat treatment as well as after machining. In the latter case, a piece of material was cut in the correspondence of the surface to catch material alterations induced by turning operations. It is worth underlining that the nanoindentation test series were conducted within a distance of 60 μm from the sample rim.

The surface topographies of the PBF-LB machined samples were captured using the 20× confocal objective of the Sensofar™ Plu-Neox optical profiler. The arithmetic mean height (S_a) was analyzed and processed as defined in the ISO 25178 standard. For each sample, three 0.66 × 1.66 mm² scans were acquired.

3. Results and discussion

3.1. Microstructure and superelastic properties before machining

The microstructures of the AB and T6 samples are shown in Fig. 3. The AB samples were characterized by an equiaxed microstructure composed of austenite with a grain size approximately equal to the hatch spacing fixed at 60 μm. After aging, the austenitic phase remains, even if the grain size becomes larger, and the intermetallic phases precipitate along the grain boundaries. The intermetallic particles are characterized by a needle-like shape and they are uniformly distributed along the matrix, as shown in Fig. 3 on the right. The EDS analysis reported in the figure reveals that Ni₄Ti₃ Ni-rich precipitates are preferentially formed after the T6 heat treatment.

Fig. 4a reports the DSC graphs of the PBF-LB samples before and after heat treatment. Narrow peaks and decreasing transformation temperatures characterized the heat-treated samples compared to the AB ones.

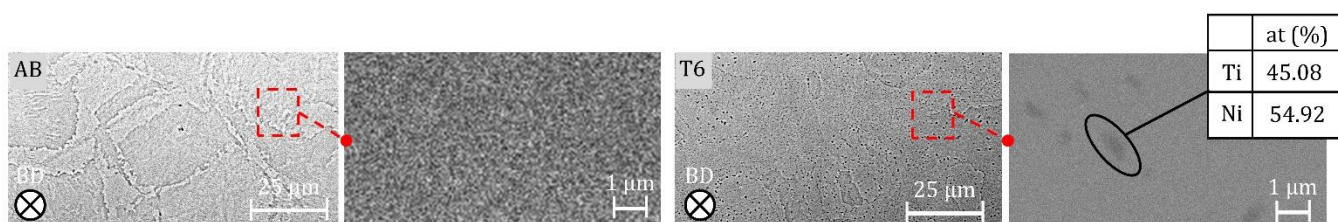


Fig. 3. Microstructure of the AB and T6 NiTi samples before machining.

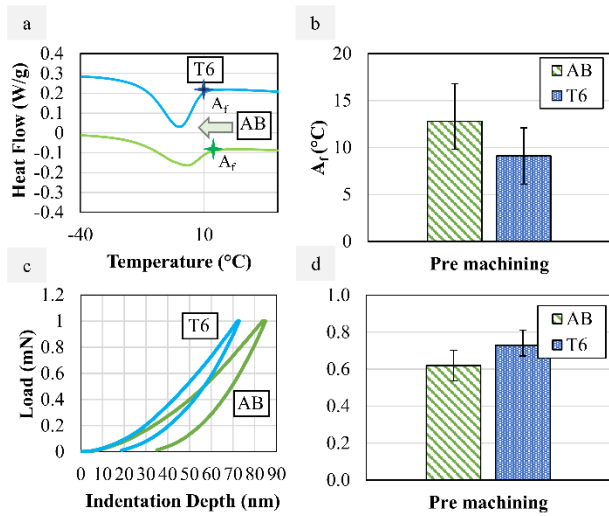


Fig. 4. a) DSC curves, b) austenite finish temperatures A_f , c) nanoindentation curves, and d) depth recovery ratio ψ before machining.

The transformation enthalpy, namely the area below the martensite/austenite transformation curve, is 57% higher for T6 samples compared to AB ones, respectively. Since the enthalpy is an indicator of the volume of transformed material, this implies that the volume fraction of material that can undergo the austenite/martensite transformation of Fig 1b is higher for the T6 samples than for the AB ones. In other words, the T6 samples are more superelastic rather than the AB ones.

Fig. 4b reports the A_f values at varying microstructural conditions. Regardless of the latter, a full austenitic state was achieved at room temperature, being always $A_f < T_{room}$. Compared to the AB case, the T6 heat treatment shifted A_f towards lower values. The decrease of A_f in the heat-treated samples can be attributed to the precipitates that were formed (see Fig. 3).

The nanoindentation curves of the samples in the AB and T6 conditions are shown in Fig. 4c, while the work recovery ratio ψ , calculated as the ratio between the recoverable deformation depth and the total one, is presented in Fig. 4d: compared to the AB condition, ψ increases by 18% after the T6 heat treatment, confirming the DSC results.

Table 1 reports the nano-hardness H value calculated from the nanoindentation curves of Fig. 4c. It can be observed that H increases by 37% after the heat treatment, because of the precipitation of fine intermetallic compounds that greatly limits the movement of dislocations [10].

Table 1. Nano-hardness H of the AB and T6 NiTi samples before machining.

AB	T6
6.58 ± 1.38	8.99 ± 1.24

3.2. Microstructure and superelastic properties after machining

Fig. 5 shows that the subsurface is characterized by the presence of a severe plastic deformed (SPD) zone, in which the grains are highly deformed towards the cutting speed direction. In general, the T6 samples are characterized by a deeper SPD layer than the AB ones. The highest the cutting speed the

thinnest the SPD layer, since the surface material is exposed to more severe temperature cycles, resulting in less strain hardening of the subsurface.

Fig. 6a reports the DSC curves after machining at $V=31$ m/min under cryogenic cooling conditions. It can be seen that machining is capable of affecting the transformation temperatures but not the shape of the curve, which remains the same before and after machining, namely narrower for the T6 samples and shallower for the AB ones.

Fig. 6b shows the A_f values at varying process parameters after machining. It can be observed that A_f increases after machining, regardless of the adopted cutting speed. This outcome can be ascribed to the martensite stabilization, induced by strain hardening generated during machining. In [11], it was demonstrated that the volume of stabilized martensite is reduced when a lower dislocation density is present in the material since the latter inhibits the reverse martensitic transformation by imposing friction stress on the martensite/parent phase.

Focusing on the effect of the cutting speed, it can be noted that the A_f is the lowest for $V=31$ m/min and the highest for $V=62$ m/min, regardless of the initial microstructural condition of the NiTi samples. In particular, the AB and T6 samples machined at $V=62$ m/min showed 28% and 33% higher A_f than the samples machined at $V=31$ m/min, respectively. At the highest cutting speed, the A_f increment was reduced by 22% only for the AB case.

This non-monotonic trend between the cutting speed and austenite transformation temperature was pointed out also in other available literature studies. In [12] the cutting force with respect to its dependence on the cutting speed and lubrication approach was studied, showing that, at low cutting speeds (i.e. $V=20$ m/min), the cutting forces were very high and the tool wear was a severe notch of the cutting edge. On the contrary, at increasing cutting speed, the cutting forces and the notch wear decreased. Specifically, when adopting a cutting speed between 60 and 130 m/min, the cutting forces were neither influenced by the cutting speed nor by the applied coolant. This is indicative of the mechanical behavior of NiTi that varies with the cutting temperature as a consequence of the cutting speed variation, as will be more detailed later.

In [13], the effects of the cutting speed on the surface integrity characteristics of a NiTi superelastic alloy ($A_f=6\pm 1^\circ\text{C}$) were investigated at varying cooling conditions (dry and cryogenic).

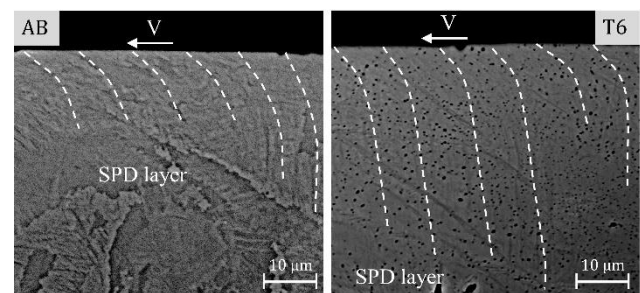


Fig. 5. Cross-section microstructure of the AB and T6 NiTi samples machined at $V=62$ m/min.

The cryogenic machining was carried out on pre-cooled samples at -185°C for 30 min, to assure the attainment of a martensitic structure throughout machining. The DSC response of the affected layers of the cryogenically machined samples shows a general increase of A_f at increasing cutting speed, with the exception of $V=50$ m/min. Again, this confirms the outcomes of the present work, namely a non-monotonic trend among the cutting temperature and A_f .

The nanoindentation curves of the samples machined at $V=31$ m/min are shown in Fig. 6c. Compared to the curves of Fig. 4a, they are shifted towards higher indentation depth values, indicating material softening after machining. The work recovery ratio ψ values reported in Fig. 6d are always lower compared to the ones before machining, confirming the SE reduction after machining as already proven by the DSC data.

Table 2 reports the nano-hardness H data at different cutting speeds. Both for the AB and T6 samples, the highest cutting speed corresponds to the highest hardness. Specifically, 7% and 12% hardness increase characterized the samples machined at $V=62$ m/min and $V=93$ m/min compared to the ones at $V=31$ m/min. Similarly, an average increase of 11% at the highest cutting speed was found for the T6 samples.

These results are not in contrast with the observations of the SPD layer reported before, since a much greater depth interested them compared to that characterizing the SPD layer.

In this work, the lowest SE characterizes the samples machined at the lowest cutting speed, contrary to what is found in many literature records (see §1).

This phenomenon can be associated with the temperature gradient that the material experiences from the surface to the subsurface during machining. Close to the surface where the cutting temperatures are the highest, it is likely that the material exceeds M_d , above which the SE is lost. In this case, the strength of the material increases at increasing temperature.

At a certain distance from the surface, when the cutting temperature is $M_s < T < M_d$, the material is cut in its austenitic state, thus presenting a superelastic behavior. In this condition, the higher the cutting speed the higher the cutting temperature, which induces higher material softening.

The latter contributes to reducing the mechanical alteration induced by machining, hence contributing to preserving the austenite phase from transforming into martensite.

Finally, at a certain distance from the surface, it is likely that the cutting temperature exceeds M_s , whose values before machining for the investigated material are reported in Table 3 so that the deformation takes place when the material is under a martensite state. Thus, according to [14], the NiTi deformation takes place when the material strength is lower compared to the austenite case.

In summary, high cutting speeds correspond to material softening, but only in the case that both the surface and subsurface temperature are above A_f but below M_d . On the contrary, if a portion of the material is cut below M_s , the material deformation becomes easier since a part of the subsurface is transformed into martensite.

The SE is strictly connected to the deformation mode, hence to the cutting temperature, since dislocations and defects formation can prevent the austenite pseudoelastic transformation of Fig. 1b. The severe temperature gradient during machining coupled with the unique behavior of NiTi can explain the non-monotonic decrease of SE with an increase in the cutting speed.

Table 2. Nano-hardness H of the AB and T6 NiTi samples after machining.

H (GPa)	AB	T6
$V=31$ m/min	4.69 ± 0.52	5.09 ± 0.24
$V=62$ m/min	5.02 ± 0.39	5.65 ± 0.71
$V=93$ m/min	5.25 ± 0.57	5.62 ± 0.50

Table 3. Martensite start temperature M_s of the AB and T6 NiTi samples before machining.

	AB	T6
M_s ($^{\circ}\text{C}$)	-7.57 ± 0.5	-17 ± 0.3

3.3. Surface finish of the machined surfaces

Analyzing the surface roughness S_a data reported in Fig. 7, it can be observed that the AB samples present an average 20% increase in S_a compared to the T6 ones.

Even if the AB samples are characterized by lower hardness and SE than the T6 ones (see Fig. 4 and Table 1), they still provoke the formation of a rougher surface. This outcome can be attributed to the inhomogeneous microstructure that characterizes the AM materials, which is governed by the melt pool boundaries, as long as unresolved residual stresses.

Given the heat treatment, the effect of the cutting speed on the S_a values reflects the same trend already found and discussed for A_f as well as ψ . Specifically, the highest S_a pertains to the samples machined at the highest cutting speed, whereas the lowest S_a to the ones machined at the intermediate cutting speed. In other words, the lower the SE the smoother the machined surface.

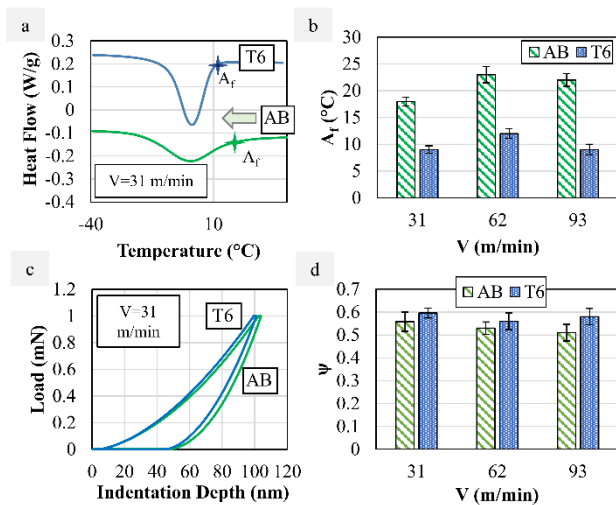


Fig. 6. a) DSC curves, b) austenite finish temperatures A_f , c) nanoindentation curves, and d) depth recovery ratio ψ after machining.

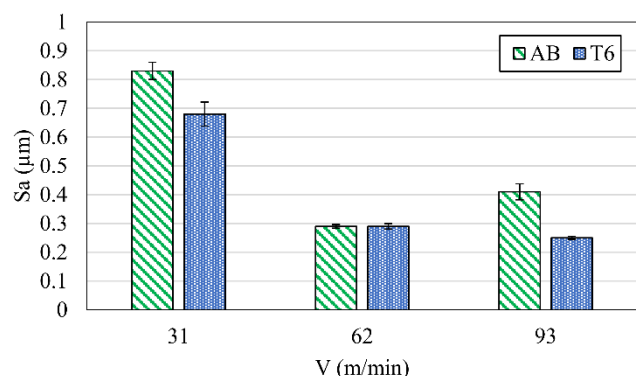


Fig. 7. Surface roughness S_a at varying cutting speeds.

4. Conclusions

To investigate the effect of the cutting speed on the surface integrity and SE, turning operations were performed on PBF-LB NiTi samples in the as-built and aged microstructural conditions. The SE was evaluated in terms of austenite finish temperature and depth recovery ratio while the surface integrity was in terms of microstructure alterations, nano-hardness, and surface roughness.

The main findings can be summarized as follows:

- The solution and aging treatment carried out on the PBF-LB NiTi samples promoted the formation of intermetallic particles as well as grain coarsening. The microstructural change is responsible for the increase of SE and hardness that characterize the heat-treated samples compared to the as-built ones.
- Regardless of the initial microstructural condition, machining was found to contribute to a decrease in the material SE and hardness. This is attributable to the martensite formation during cutting, which decreases the amount of austenite that can undergo the pseudoelastic transformation.
- A non-monotonic trend between the cutting speed and SE was highlighted, since, given the adoption of cryogenic cooling, the material can experience a temperature gradient from the machined surface to the subsurface, to which corresponds a drastic change in the material's mechanical behavior.
- To higher cutting speed corresponds to the formation of harder surfaces since the austenitic phase has higher yield strength compared to the martensitic one.
- AB samples, despite having lower hardness and SE than T6 samples, show a 20% increase in surface roughness due to the inhomogeneous microstructure typical of PBF-LB manufactured materials.
- Higher cutting speeds lead to increased surface roughness, with the highest S_a values observed in samples machined at the highest speed, and the lowest at intermediate speed. Essentially, a lower SE correlates with a smoother machined surface.

Future works will be focused on investigating the long-term performance and fatigue resistance of the PBF-LB heat-treated and machined NiTi samples.

Acknowledgments

This work was financially supported by PNRR research activities of the consortium “iNEST (Interconnected North-East Innovation Ecosystem)” funded by the European Union Next-GenerationEU (Piano Nazionale di Ripresa e Resilienza (PNRR) – Missione 4 Componente 2, Investimento 1.5 – D.D. 1058 23/06/2022, ECS_00000043) and by the PRIN project “NEMESI - 4D manufacturing based on 3D printing and machining for Nitinol biomedical and sensing applications” funded by the Italian Ministry of University and Research (MUR).

References

- [1] Weinert K, Petzoldt V, Kötter D. Turning and drilling of NiTi shape memory alloys. *CIRP Annals Manuf Technol* 2004;53(1):65-68.
- [2] Guo Y, Klink A, Fu C, Snyder J. Machinability and surface integrity of Nitinol shape memory alloy. *CIRP Annals: Manuf Technol* 2013;62(1):83-86.
- [3] Yang H, Sakai K, Shizuka H, Kurebayashi Y, Hayakawa K, Nagare T. Effect of cutting speed on shape recovery of work material in cutting process of super-elastic NiTi alloy. *Int J Autom Technol* 2021;15(1):24-33.
- [4] Yang H, Sakai K, Shizuka H, Kurebayashi Y, Hayakawa K, Nagare T. Experimental investigation of the effects of super-elasticity on the machinability of NiTi alloys. *Int J Adv Manuf Technol* 2021;115(1-2):581-593.
- [5] Kaynak Y. Machining and phase transformation response of room-temperature austenitic NiTi shape memory alloy. *J Mater Eng Performance* 2014; 23:3354-3360.
- [6] Kaynak Y, Karaca HE, Noebe RD, Jawahir IS. Analysis of tool-wear and cutting force components in dry, preheated, and cryogenic machining of NiTi shape memory alloys. *Procedia CIRP* 2013;8:498-503.
- [7] Bertolini R, Bruschi S, Ghiotti A, Savio E, Ceseracciu L, Jawahir IS. Surface integrity and superelastic response of additively manufactured Nitinol after heat treatment and finish machining. *CIRP Annals: Manuf Technol* 2023;72(1):501-4.
- [8] Khademzadeh S, Zanini F, Rocco J, Brunelli K, Bariani PF, Carmignato S. Quality enhancement of microstructure and surface topography of NiTi parts produced by laser powder bed fusion. *CIRP J Manuf Sci Technol* 2020;31:575-582.
- [9] Bruschi S, Bertolini R, Ghiotti A, Savio E, Guo W, Shivpuri, R., 2018, Machining-induced surface transformations of magnesium alloys to enhance corrosion resistance in human-like environment *CIRP Annals: Manuf Technol* 2018; 67(1):579-82.
- [10] Bai Y, Zhao C, Yang J, Hong R, Weng C, Wang H. Microstructure and machinability of selective laser melted high-strength maraging steel with heat treatment. *J Mater Process Technol* 2021;288:116906.
- [11] Olbricht J, Yawny A, Condó AM, Lovey FC, Eggeler G. The influence of temperature on the evolution of functional properties during pseudoelastic cycling of ultra fine grained NiTi. *Mater Sci Eng: A*, 2008;481:142-5.
- [12] Kowalczyk M. Cutting forces during precise turning of NiTi shape memory alloy. *Czasopismo Techniczne*, 2017;7:137-146.
- [13] Kaynak, Y. U. S. U. F., Karaca, H. E., & Jawahir, I. S. (2015). Cutting speed dependent microstructure and transformation behavior of NiTi alloy in dry and cryogenic machining. *Journal of Materials Engineering and Performance*, 24, 452-460.
- [14] Benafan O, Noebe RD, Padula Ii SA, Gaydos DJ, Lerch BA, Garg A, Vaidyanathan R. Temperature-dependent behavior of a polycrystalline NiTi shape memory alloy around the transformation regime. *Scripta Mater* 2013;68(8):571-4.